Earthquakes and Structures, *Vol. 17, No. 4 (2019) 373-385*
DOI: https://doi.org/10.12989/eas.2019.17.4.373

Different approaches for numerical modeling of seismic soil-structure interaction: impacts on the seismic response of a simplified reinforced concrete integral bridge

Sreya Dhar*[1], Ali Güney Özcebe[2,3a], Kaustubh Dasgupta[1b], Lorenza Petrini[2b] and Roberto Paolucci[2b]

[1]*Department of Civil Engineering, Indian Institute of Technology, Guwahati, 781039, India*
[2]*Department of Civil and Environmental Engineering, Politecnico di Milano, Milano, 20133, Italy*
[3]*Department of Civil Engineering and Architecture, Università di Pavia, Pavia, 27100, Italy*

(*Received May 28, 2019, Revised August 12, 2019, Accepted August 21, 2019*)

Abstract. In this article, different frequently adopted modeling aspects of linear and nonlinear dynamic soil-structure interaction (SSI) are studied on a pile-supported integral abutment bridge structure using the open-source platform OpenSees (McKenna *et al*. 2000, Mazzoni *et al*. 2007, McKenna and Fenves 2008) for a 2D domain. Analyzed approaches are as follows: (i) free field input at the base of fixed base bridge; (ii) SSI input at the base of fixed base bridge; (iii) SSI model with two dimensional quadrilateral soil elements interacting with bridge and incident input motion propagating upwards at model bottom boundary (with and without considering the effect of abutment backfill response); (iv) simplified SSI model by idealizing the interaction between structural and soil elements through nonlinear springs (with and without considering the effect of abutment backfill response). Salient conclusions of this paper include: (i) free-field motions may differ significantly from those computed at the base of the bridge foundations, thus put a significant bias on the inertial component of SSI; (ii) conventional modeling of SSI through series of soil springs and dashpot system seems to stay on the safer side under dynamic conditions when one considers the seismic actions on the structure by considering a fully coupled SSI model; (iii) consideration of abutment-backfill in the SSI model positively affects the general response of the bridge, as a result of large passive resistance that may develop behind the abutments.

Keywords: soil-structure interaction; numerical seismic analysis; integral bridge

1. Introduction

Over the last few decades, integral bridges (IBs) have become popular due to their easy attributes of construction, low maintenance cost, easy to retrofit (Mirrezaei *et al*. 2016, Dhar and Dasgupta 2019a) and high durability over service life (Greimann *et al*. 1986, Horvath 2000, Arockiasamy *et al.* 2004, Conboy and Stoothoff 2005, Weakley 2005, Petursson and Kerokoski 2011, Argyroudis *et al*. 2016, Mitoulis *et al*. 2016, Kim *et al*. 2018, Dhar and Dasgupta 2019b). Since integral (or jointless) bridges have no bearing or energy dissipating devices installed throughout the structure, unlike the conventional bridges (Wasserman and Walker 1996), the overall movement of superstructure and rotation of abutments and foundation have to be accommodated through soil-pile interaction and abutment-backfill interaction as a single unit (Lee *et al*. 2016, Park and Nam 2018, Tsinidis *et al*. 2019). Hence, design and detailing of IBs are quite challenging, while balancing the forces and moments at abutment and deck integral connection.

A schematic diagram of a two-span, pile-supported IB is illustrated in Fig. 1, where it is worth mentioning that single rows of piles are often present under the abutments helping principally the bending around the weak direction (Arockiasamy *et al*. 2004, Arsoy *et al*. 2002, Quinn and Civjan 2016) and reducing the unequal soil settlements at abutment locations, thus mitigating an important vulnerability as large rotations that might not be accommodated by internal deck-pier joints.

It is generally accepted in the earthquake engineering practice that the role of dynamic soil-structure interaction (SSI) in the seismic response of structures is overall beneficial because it tends to reduce the seismic demand on the structure (Karakas *et al*. 2018, Messioud *et al*. 2016). For this reason, seismic analysis of structures is often carried out either with no consideration of such effects, i.e., considering an infinitely rigid foundation soil, or with simplified models representing the soil-foundation-structure interaction (SSI) through lumped mass, linear/nonlinear springs and dashpots coefficients (e.g., Gazetas 1991, Ali and Kim 2017, Ganjavi *et al.* 2018, Guo *et al*. 2016). To consider nonlinear SSI of bridge-foundation system, simplified models with spring-dashpots has been numerically adopted in the past (e.g., Zhang and Makris 2002, Finn 2004, Ostadan *et al*. 2004, Kotsoglou and Pantazopoulou 2009, Hoseini *et al*. 2019, Dhar and Dasgupta 2019c).

∗Corresponding author, Former Ph.D. Student
E-mail: sreya.dhar@gmail.com
[a]Joint Post-Doctoral Research Associate
[b]Professor

http://www.techno-press.com/journals/eas&subpage=7
ISSN: 2092-7614 (Print), 2092-7622 (Online)

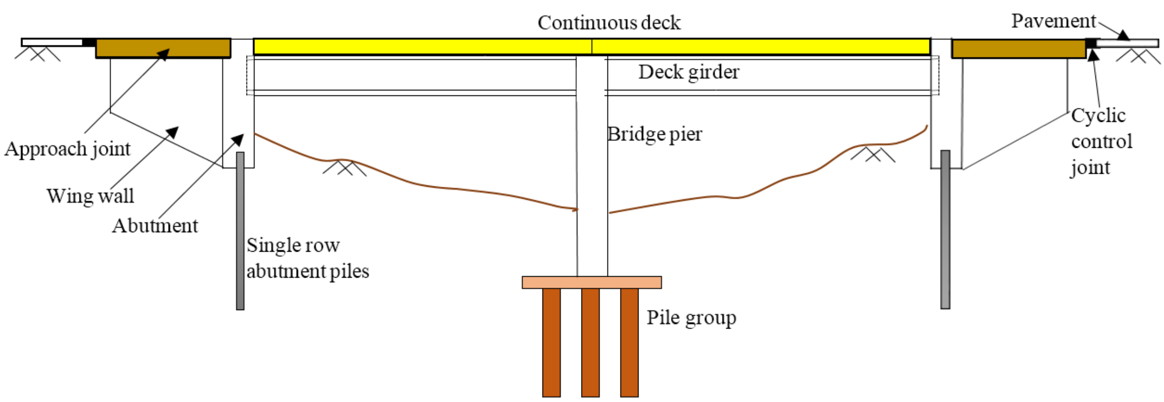

Fig. 1 General schematic diagram of a two-span pile supported integral bridge

Recently, displacement-based studies have been carried out on similar modeling assumptions (Paolucci *et al*. 2013, Ahmadi *et al*. 2015) to incorporate nonlinear SSI in the soil-foundation system. Only very seldom the non-linear dynamic soil-foundation-structure interaction has been considered in the numerical modeling of the problem (Naderi and Zekavati 2018, Jiang *et al*. 2018), although it is proved in many past researches to affect significantly the overall structural response (e.g., Clough and Penzien 2003, Boulanger *et al.* 1999, Figini and Paolucci 2017).

Creation of fully coupled models including soil, foundation, and structure, properly accounting for their non-linear behavior, requires significant expertise in both numerical modeling of soils and structures, in addition to the significant increase of the computational cost. Therefore, the practice on this fully coupled approach is commonly used only for important bridges (Shamsabadi *et al.* 2007, Zhang *et al*. 2008, Elgamal *et al.* 2008, Elgamal 2010). Under the high intensity of shaking, due to abutment backfill interaction, bridge's overall damping and vibration period increase (Douglas and Reid 1982, Goel 1997). The additional damping occurs due to the inelastic behavior of the backfill soil (Caltrans 2013, Mitoulis 2016).

Mainly focusing on the typology of IB system due to previously mentioned potential vulnerabilities, the effect of SSI on IB structural typology has been studied through the use of dynamic impedances (Carvajal 2011, Thanoon 2011, Karantzikis and Spyrakos 2000, Zhao 2011, Erhan and Dicleli 2017) and found out to be beneficial. As also mentioned earlier, up to the authors' knowledge, there is still a lack of information on the complete response that could only be obtained through coupled nonlinear soil-structure models. Besides, the impact on the overall structural response of different modeling assumptions of the SSI, encompassing the nonlinearities of the soil response and the soil-foundation interaction, still deserves additional clarification.

The objective of the present study is to compare the response of IB from different modeling approaches performed in dynamic response analysis; to provide an overview on differences in bridge response via suitable parameters and to prescribe the most appropriate modeling approach to study multi-span IB considering its structural intricacies.

2. Numerical modeling

The present study provides six different modeling approaches encompassing various assumptions and boundary conditions which are adopted in the current day practice (Table 1). All the models were created and analyzed by using the OpenSees platform (McKenna *et al.*, 2000, Mazzoni *et al*. 2007, McKenza 2008). Linear and non-linear time-history analyses (THA) were performed with a focus on the longitudinal response of the bridge. Due to excellent documentation available in the literature, on the structural configuration, soil formation and seismic response of the Humboldt Bay Middle Channel (HBMC) Bridge (Zhang *et al*. 2008, Elgamal *et al.* 2008), in this paper a modified and simplified version of this structure was taken into consideration, by excluding on purposely shear keys and expansion joints present at the superstructure level to resemble an IB system and removing the curved geometry at the deck level to make the overall geometry of the superstructure more commonly observed. Details regarding the structural modeling, geotechnical modeling, and soil-structure interaction modeling are provided in Sections 2.1, 2.2, and 2.3; respectively.

2.1 Structural modelling

Bridge model under consideration was 330 meters long, 12 meters tall, and 10 meters wide with monolithic connections at the pier/abutment-superstructure level (Dhar 2018, Dhar *et al*. 2017). The superstructure consisted of nine equal spans, stiffness of which is given by four precast prestressed concrete I-girders and cast-in-place concrete slabs. Beneath the piers, driven precast pile group with their pile caps were taken into consideration, as well. As mentioned in Table 1, the very same structure was modeled by using both linear beam-column elements (in M1L, M2L, M3L, and M3NL-2) and nonlinear force-based elements (in M1NL, M2NL, M3NL-1, M3NL-3, M4, M5, and M6).

Properties of structural elements for linear analyses were adopted from Zhang *et al.* (2008) as A (area in m^2)=12, 4.56, 3.4 and I (moment of inertia in m^4)=1.44, 3.212, 0.8188 for the abutment, deck (superstructure) and pier sections, respectively. All the same elements shared the same concrete elastic modulus of 28 GPa, thus excluding the effect of concrete

Table 1 List of models used in the analyses

Model	Sub-model	SSI approach: Foundation	SSI approach: Abutment	Modeling approach: Structural	Modeling approach: Soil	Input motion	Scheme
M1	M1L	Fixed	Free	Linear beam-column elements	Does not exist	Free-field motion applied from the base of piers and abutments	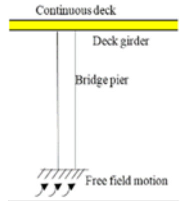
	M1NL			Nonlinear fiber elements			
M2	M2L	Fixed	Free	Linear beam-column elements	Does not Exist	Ground surface motion obtained from M3-L and M3-NL	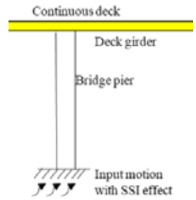
	M2NL			Nonlinear fiber elements			
M3	M3L	Coupled SSI	Free	Linear beam-column elements	Linear quad elements	1D incident motion is applied from the model base at bedrock level depth	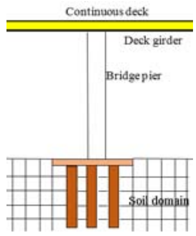
	M3NL-1			Nonlinear fiber elements	Nonlinear quad elements		
	M3NL-2			Linear beam-column elements	Nonlinear quad elements		
	M3NL-3			Nonlinear fiber elements	Linear quad elements		
M4		Coupled SSI (as above)	Coupled SSI	Nonlinear fiber elements	Nonlinear quad elements	1D incident motion is applied from the model base at bedrock level depth (as above)	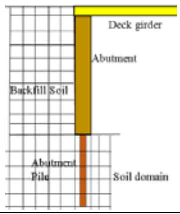
M5		Springs and dashpots according to API-rp2a (2000); Gazetas and Dobry (1984)	Free	Nonlinear fiber elements	Does not Exist	Free-field motion applied at spring ends	Details in Fig. 4
M6		Springs and dashpots (as above)	Springs defined according to Highway Agency (2003) (working only under compression)	Nonlinear fiber elements	Does not Exist	Free-field motion applied at spring ends (as above)	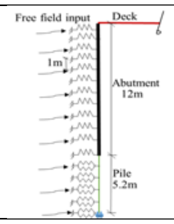

cracking in the linear models.

In the nonlinear simulations, on the other hand, force-based elements (Neuenhofer and Filippou 1998) with 10 integration sections were used for piers. Abutments and piles are kept linear elastic. Material properties used in the study for piers were adapted from Zhang *et al*. 2008. The cross-section is discretized into three fiber sub-regions: confined and unconfined concrete and rebar (Fig. 2(a)) Kent-Park-Scott (Scott *et al*. 1982) concrete model was used to describe nonlinear concrete material behavior with degraded linear unloading/reloading stiffness and zero tensile strength. Compressive strengths of confined and unconfined concrete were 34.5 MPa and 27.6 MPa, respectively. Giuffre-Menegotto-Pinto (Filippou *et al*. 1983) steel material model, with 200 GPa elastic modulus, 276 MPa yield strength and 0.8% isotropic strain hardening, was adopted for reinforcement bars.

All the models containing the foundation (i.e., M3 to M6), actual reinforced concrete groups with pile cross-section shown in Fig. 2(b) were simplified and modeled as elastic equivalent pile group according to Ariyarathne *et al*. (2013). A Rayleigh damping model was introduced for viscous damping forces in the linear and nonlinear time history analyses. The damping ratio was prescribed as 5% at 0.5 Hz

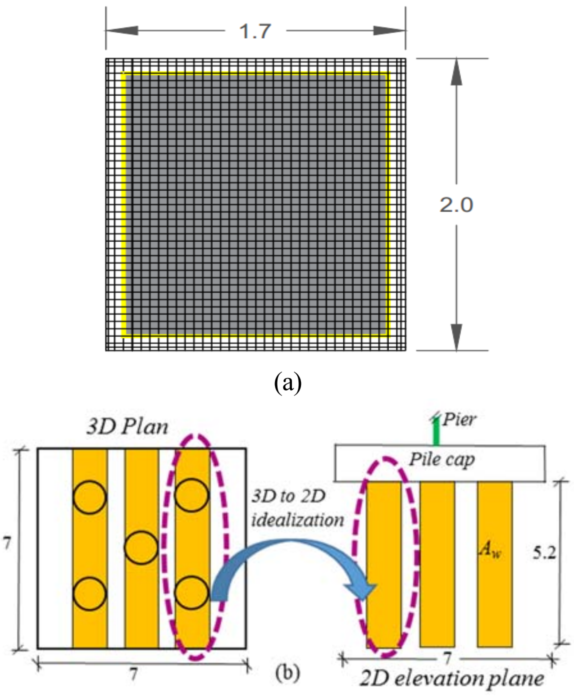

(b)

Fig. 2 (a) Nonlinear model: piers cross-section is discretized into 20×20 fibers; in grey the confined concrete fibers, in yellow the reinforcement fibers and in white the unconfined concrete fibers, (b) equivalent pile group projection from 3D to 2D; where A_w=equivalent effective area considered in 2D; this is the zoom-up window of pile foundation from the global model shown in Fig. 3(b). All dimensions in m. (not to scale)

and 5.0 Hz for all of the models.

2.2 Geotechnical modeling

A two-dimensional soil modeling was adopted. Soil domain was 1500 meters wide (iteratively evaluated to obtain free-field motion at the boundary) and 220 meters in depth (Fig. 3(a)). Whole soil domain consisted of 4 different layers having the static and dynamic properties summarized in the table present in Fig. 3(d), in which the geotechnical constitutive parameters were adapted from Zhang *et al.* (2008). Pressure independent multi-yield material was used to describe the soil behavior through a formulation based on the multi-surface, nested plasticity concept (Prevost 1985) with associated flow rule. The yield surfaces were of the Von Mises type. Since total stress analyses were carried out, thus any direct consequence of significant excess pore water pressure generation was implicitly neglected. To represent the hysteretic response of the soil elements, a degradation of the shear modulus was considered according to Darendeli (2001), as shown in Fig. 3(c) and the soil damping, is automatically captured by the code according to the constitutive law under consideration. Hysteretic damping due to stress-strain reversals, on the other hand, was inherently captured by the nested plasticity constitutive model.

The mesh dimension was constrained so that elastic seismic waves can accurately propagate with a maximum frequency of 15 Hz under linear conditions. Accordingly, soil mesh (Fig. 3(b)) is reduced moving from bottom to top

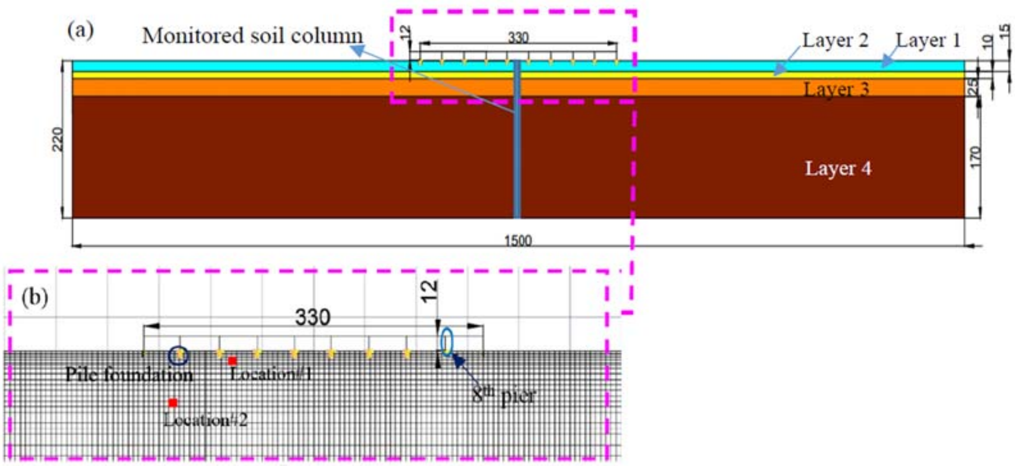

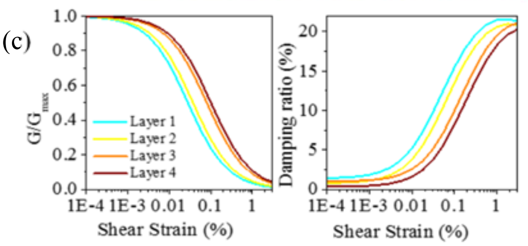

(d)

Soil layer	Elastic properties			
	Maximum shear modulus (MPa)	Poisson's ratio	Total unit weight (t/m^3)	Shear modulus ratio (Fig. 3c)
Layer 1	76	0.40	1.9	Cyan Line
Layer 2	171	0.40	1.9	Yellow Line
Layer 3	288	0.40	1.8	Orange Line
Layer 4	525	0.40	2.1	Brown Line

Fig. 3 (a) Two-dimensional soil domain with 4 layers, dimensions are in meters. The monitored soil is used to investigate the effects of the presence of structure on the soil response (see Section 4). (b) Details of the mesh in the bridge-soil-interaction zone. For the marked soil elements, linear/nonlinear response will be discussed in detail in Section 4. (c) Shear modulus degradation and shear damping ratio curves. (d) Table with the properties of different soil layers. It is noted that layer colors are kept same in (a), (c), and (d) from 5 m to 1m length ($L_{max}=V_s/8f_{max}$, where L_{max} is the maximum length of soil mesh, V_s is the mean shear wave velocity and f_{max} is the maximum frequency to be propagated by the soil mesh (Kuhlemeyer and Lysmer 1973)). A soil column (Fig. 3(a)) in the middle of the domain is selected for monitoring the strain and acceleration response for linear and nonlinear SSI models.

2.3 Soil-structure interaction modeling

Soil-structure interaction was considered in models M3, M4, M5, and M6, with an idealization of foundation group in Section 2.1. In M3, the full coupling of SSI is considered only at the foundation level, while in M4 it was also present between the abutment and backfill soil (Table 1). In both the cases, structural and soil elements in contact were glued to each other without permitting any nonlinear response neither as gapping nor as sliding along their interface.

In models M5 and M6, group effect was reflected through proper p-multiplier calculated according to Mokwa (1999), which was considered on an average of 0.65 under cyclic loading. Soil-pile interaction was modeled by zero-length spring-dashpots to represent the near and far-field soil domain. In the near field soil, hysteretic damping was considered due to the nonlinearity of spring materials. Lateral and vertical springs were modeled from API-rp2a (2000) in parallel to each other to represent lateral load-bearing capacity and skin friction of pile surface, respectively. Far-field soil stiffness and radiation damping were modeled through springs and dashpots in parallel, using the spring stiffness and damping coefficients provided in Gazetas and Dobry (1984) and positioned in series with near-field nonlinear hysteretic springs. A scheme of the spring-dashpot system is reported in Fig. 4. It has been proven from past researches that API force-displacement relationships overestimated the soil stiffness (Granas 2016, Brødbæk *et al.* 2009, Monkul 2008). Thus, to make a rational comparison, 5% RD is also considered in the "simplified models" with spring-dashpots (Zhang and Makris 2002, Ahmadi *et al*. 2015).

In M6, nonlinear springs were also added to model the abutment backfill soil. A frame-type abutment was considered, and nonlinear springs were positioned at 1 m distance along the length of the abutment wall (Table 1). Parameters for the nonlinear force-deformation curves were calculated according to Highway Agency (2003).

2.4 Boundary conditions and application of input motion for dynamic analyses

The boundary conditions and dynamic input applied to different models were explained in the following list:

1. For M1: Pier and abutment ends were clamped. Free-field motion (computed at the soil surface) was applied as acceleration time histories at foundation level.

2. For M2: Pier and abutment ends were clamped. Different than M1, the input acceleration motion was calculated by M3L/NL at foundation level.

3. For M3 and M4: There were no boundary conditions applied directly to the structural elements. Soil domain extreme lateral sides were tied degrees of freedom (TDOF) (Elgamal *et al.* 2008, Kontoe *et al.* 2007) that follows the horizontal free-field motion of a 1D soil column. At the base level, instead, Lysmer and Kuhlemeyer (1969) type absorbing boundary conditions were applied in the horizontal direction by properly calibrating the dashpot coefficients together with the classical vertical displacement restraints. Input motion field was applied from the bottom in terms of upward propagating shear stress that corresponds to the free-field incident velocity field of the rock outcrop.

4. For M5 and M6: Horizontal free-field motion was applied at the end of exterior interaction springs (see Table 1 and Fig. 4).

As it could be pointed from the points from 1 to 4, all the models apart from M3 and M4, require a set of pre-determined free-field motions at desired elevations. To cope with this issue, preliminary 1D soil column analyses were carried out by keeping the same geotechnical modeling assumptions made in Section 2.2 and boundary conditions stated in Point 3.

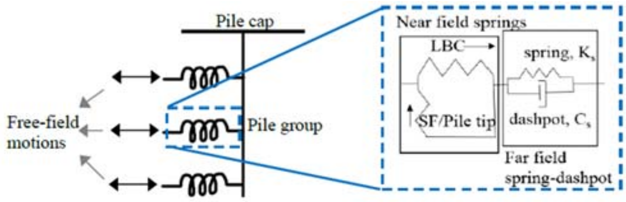

Fig. 4 Scheme of the spring-dashpot system used for describing soil-pile interaction in M5 and M6. LBC=Lateral Bearing Capacity; SF=Skin Friction; K_s=spring stiffness; C_s= damping coefficient

3. Selection of ground motions

A bedrock uniform hazard response spectrum (UHRS) was used to select input motions for the analyses which have been discussed in Dhar *et al.* (2016). The UHRS was developed from the 2008 United States Geological Survey (USGS) (Petersen *et al.* 2008) national seismic hazard maps for the Humboldt Bay area for rock outcrop assuming $V_{S,30m}$=800 m/s (according to NEHRP (Holzer *et al.* 2005), USGS site class B). The corresponding 5% damped elastic displacement response spectrum was given as target to REXEL-Disp (Smerzini *et al.* 2012) to select and scale the ground motions for dynamic analysis from strong ground motion database SIMBAD (Smerzini *et al.* 2014). The input parameters in REXEL-Disp to find the ground motions were: magnitude=5.5-7.5; fault to site distance=0-30 km; spectrum matching tolerance=±20%; spectrum matching period=0.2-5 s; site specification=EC8 site class A (which covers A and B of USGS classification); probability of exceedance=10% in 50 years. Seven real record ground motions were chosen for horizontal direction by scaling in the response spectrum around the period of interest, such that the mean spectral response lied between the tolerances. Different parameters of selected ground motions (GM) and scaling factors were summarized in the table reported in Fig. 5(a). The corresponding 5% damped elastic

Earthquake Name	Date	M_W	Epicentral distance (km)	PGA (m/s^2)	Scale Factor	Scaled PGA (m/s^2)
Irpinia	23 Nov 1980	6.9	23.8	0.54	6.31	3.46
South Iceland	17 June 2000	6.5	5.3	3.39	0.90	3.06
Olfus	29 May 2008	6.3	8.3	3.28	1.67	5.47
Olfus	29 May 2008	6.3	8.0	5.00	1.41	7.06
Irpinia	23 Nov 1980	6.9	28.3	0.95	0.72	0.68
South Iceland	21 June 2000	6.4	22.0	0.51	1.42	0.73
Christchurch	21 Feb 2011	6.2	1.5	9.16	1.38	12.64

(a)

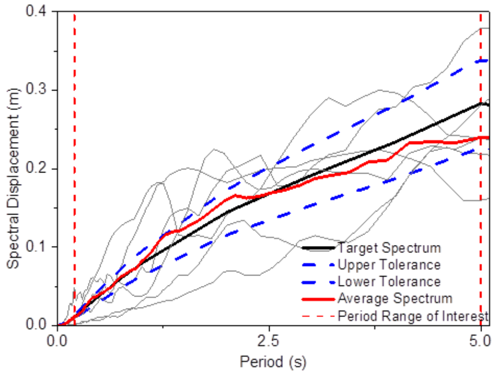

(b)

Fig. 5 (a) Scaled rock outcrop motions and (b) their spectral match with target uniform hazard response spectrum

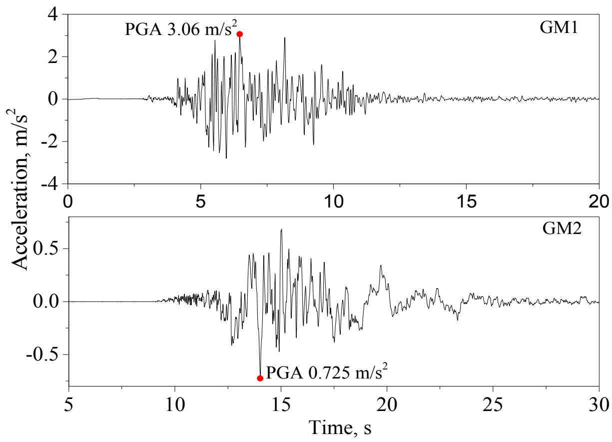

(a)

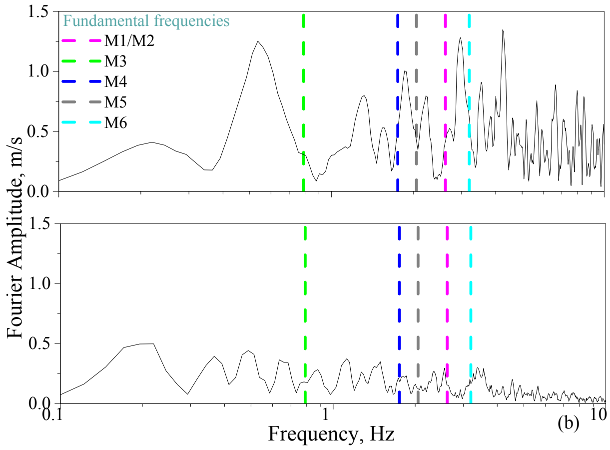

(b)

Fig. 6 (a) Acceleration response of South Iceland earthquakes registered 17 (GM1) and 21 (GM2) of June in time and (b) frequency domains. The fundamental frequencies of the models are overlapped on (b): $f_{1,M1\&M2}$=2.62 Hz, $f_{1,M3}$=0.79 Hz, $f_{1,M4}$=1.75 Hz, $f_{1,M5}$=2.06 Hz, $f_{1,M6}$=3.2 Hz

displacement spectra with the average of the ground motions were plotted in Fig. 5(b).

Two of the six ground motions reported in Fig. 5 (highlighted in grey in the table), i.e., South Iceland earthquakes registered the 17th (GM1) and 21th (GM2) of June 2000, were particularly interesting because they correspond to same soil profile (i.e., same station), similar magnitudes but different intensities due to their difference in source to site distances. The time and frequency domain acceleration plots of these specific records were provided in Fig. 6. Aiming to identify how different levels of complexity in modeling may affect computational results, these two input motions have been used to compare the structural responses of the six models. In Section 4, the obtained results were presented, highlighting similarities and differences. Given the significance of the current work on the modeling of soil-structure interaction, at first, the response of the soil domain was investigated (Sec 4.1) and, then, its effects on the structure was presented (Sec 4.2).

In Section 5, mean structural responses due to all inputs were also analyzed and discussed in the scope of a seismic code-based approach which required the average response emerging from a set of time history analyses.

4. Geotechnical and structural dynamic response under GM1 and GM2

4.1 Geotechnical dynamic response

In this section, the nonlinear response of the soil domain was synthesized through comparisons of (i) stress-strain loops recorded at positions shown by red in Fig. 3(b) and (ii) peak acceleration/strain profiles recorded at the soil elements shown by the blue soil column in Fig. 3(a). For both comparisons, the results of model M3 were used. Stress-strain responses of the tracked soil elements were shown in Fig. 7.

It could be understood from Fig. 7 that soil elements located closer to surface suffered from a greater amount of nonlinearity as compared to their deeper counterparts located at 34 m. This was an expected outcome due to reduced soil strength at shallower depths and further nonlinearities induced due to dynamic soil-structure interaction at foundation level. Furthermore, the induced level of nonlinearity due to GM1 (Fig. 7(a) and 7(c)) was considerably higher when compared to the level of nonlinearity caused by GM2 (Fig. 7(b) and 7(d)), especially at both shallower and deeper locations. It could be summarized that under the effect of both GM1 and GM2, there existed nonlinear soil responses at both locations but with decreasing trends with increasing depth (i.e., fatter

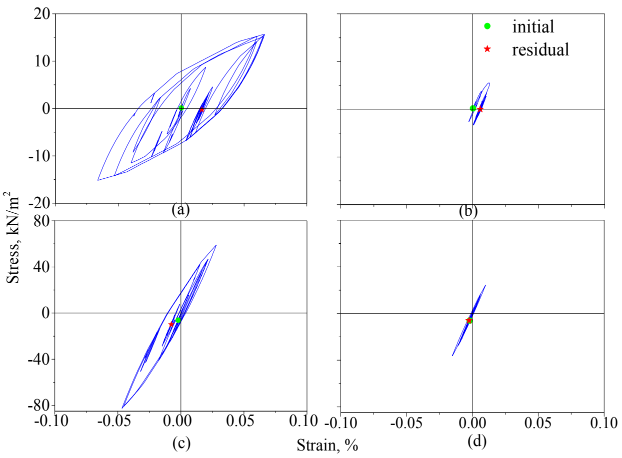

Fig. 7 Shear stress-shear strain responses at Location#1 (L1) and Location#2 (L2): (a) L1 under GM1, (b) L1 under GM2, (c) L2 under GM1, (d) L2 under GM2

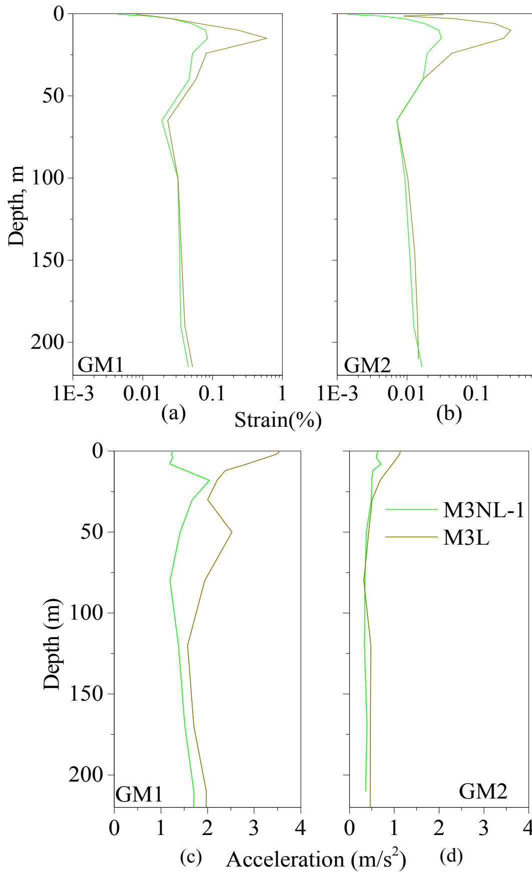

Fig. 8 Peak response profiles for the soil elements of the soil column presented in Fig. 3 by using the nonlinear soil (M3NL-1) and linear soil hypotheses (M3L): (a) shear strain (%) profiles under GM1, (b) shear strain profiles (%) under GM2, (c) acceleration profiles (m/s^2) under GM1, (d) acceleration profiles (m/s^2) under GM2

loops and higher residual strains at the shallower point, Fig. 7(a) and 7(b)) and decreasing intensity (i.e., thinner loops and smaller residual strains under GM2-Fig. 7(b) and 7(d)). To investigate the level of nonlinearity as a function of depth, one can plot peak strain and acceleration profiles

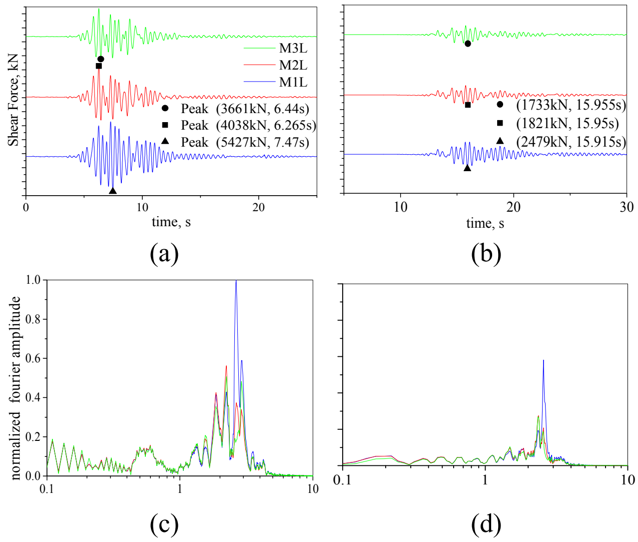

Fig. 9 The shear force from linear TH analyses. (a) GM1, (b) GM2, normalized Fourier transform of shear force THs under (c) GM1 and (d) GM2

computed through the results of sub-models M3L and M3NL-1. This comparison was presented in Fig. 8.

It could be commented on Fig. 8(a) and 8(b) that the maximum depth from which the effects of nonlinear soil response were visible around 100 meters under GM1 and 40 meters under GM2, with a well visible region until 25 meters of depth. Given the fact that the length of the pile foundations was short, it could be explained that for only first 10-15 m there was the influence of nonlinear SSI mechanism, below which the nonlinear response of horizontally deposited soil layers played the major role. Again, from Fig. 8(b) it could be mentioned that there was a trend of increasing strain in the results of M3NL-1 for the superficial depths under 3 m, which likely shows the nonlinearity caused due to the event dependency of GM2. Thus, an additional amount of soil damping was expected for GM2, for superficial locations.

When one investigates the peak acceleration plots (Fig. 8(c) and 8(d)), it could be noted under linear soil domain (M3L) there was a general trend of increase by decreasing depth both under GM1 and GM2. This increase was due to classical wave propagation essentials, having the constructive interference of the incident and surface reflected waves. Further decomposition of the nonlinear response could be made for depths until around 10 m (where the pile-soil interaction effect is present) and depths greater than 10 m. For the former, more or less a constant peak acceleration was observed due to the additional strengthening provided by the structural elements to the yielded soil elements, whereas for the latter there was a decreasing trend when the level of nonlinearities was high (i.e., depths between 15-25 m) and a more moderate increase when the level of nonlinearities was more moderate (i.e., depths greater than 25 m). As a final point, one might recognize slight reduction of peak horizontal acceleration at large depths~220 m between two models, this was due to slight localization of soil non-linearity at the onset of seismic wave propagation induced as shear stress.

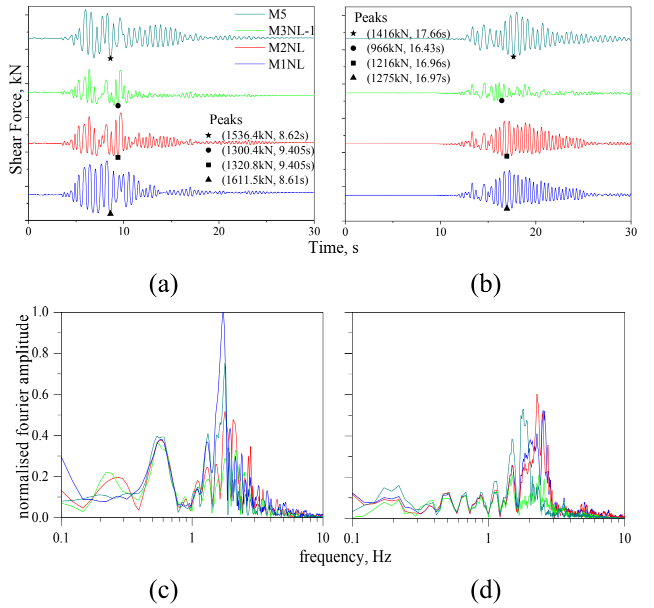

Fig. 10 Shear force from nonlinear TH analyses under (a) GM#1, (b) GM#2, normalized Fourier transform of shear force THs under (c) GM1 and (d) GM2

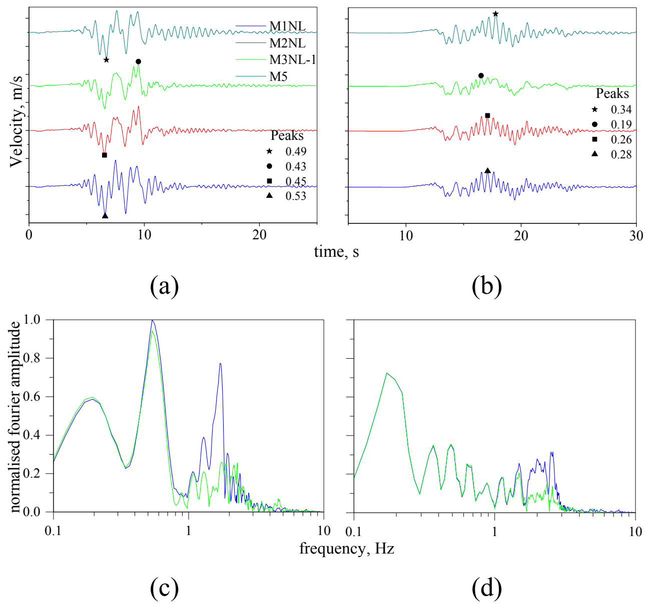

Fig. 11 Velocity time histories (VTHs) at the top of the 8th pier from NTHA under (a) GM1, (b) GM2; normalized Fourier amplitude of VTHs under (c) GM1 and (d) GM2

4.2 Structural dynamic response without the presence of the abutments-backfill interaction

As a first step, a comparison between the results of linear models M1L, M2L and M3L were performed. Particular attention was paid on pier shear force-time histories (TH). For the sake of clarity, all the results discussed in this section referred to Pier 8 resulting in the most critical one in terms of internal actions induced by GM1 and GM2. Indeed, it had been found out that the edge piers, being close to stiff abutments, suffered from higher actions.

Fig. 9(a) and 9(b) show the shear force THs for the three different models under GM1 and GM2, respectively. As expected, the highest forces were registered in M1L model (blue line), due to the combined effect of restraints at pier ends and free field motion. On the contrary, M2L model (red line), even if with fixed base columns, had a similar response of M3L (green line). This point indicated that the linear response of the bridge-soil system was governed by the inertial response of the bridge itself, rather than the kinematic interaction between the superficial foundation system and surrounding soil.

From Fig. 9(a) and 9(b), it was also visible that the M2L and M3L model peaks were almost synchronous and very similar (e.g., 4038 kN at 6.265 s and 3661 kN at 6.44 s, under GM1), while the higher M1L peak was slightly shifted at (e.g., 5427 kN at 7.47 s, under GM1). This was coherent with the normalized Fourier transform (FT) of the shear force TH (Fig. 9(c) and 9(d)), showing the highest frequency content for M1L model, with a quite sharp and shifted peak compared to other two models.

In Fig. 10, a similar type of comparison was made for the nonlinear responses (i.e., models M1NL, M2NL, M3NL-1, and M5). It could be inferred from Fig. 10(a) and 10(b) that due to material nonlinearity in piers and, in case, in foundation soil, seismic energy dissipation occurred. Nonlinear piers attracted less amount of seismic forces; thus, the response on the bridge got reduced. The peak response for the cases M1, M2 and M3 reduced by 65-70% from linear to nonlinear THA under GM1 and 30-55% for GM2.

Comparing normalized FT of the shear force TH under GM1 in linear and nonlinear THA (Fig. 9(c) vs. 10(c)), it was possible to notice a shift of the peak amplitude from the range 2-3 Hz to 1-2 Hz, for M1 and M2, due to the higher deformability of nonlinear models and a similar trend for M5. M3 showed an intensity reduction and an important shift of the maximum peak from 2.24 Hz to 0.54 Hz moving from LTHA to NTHA. On the other hand, when the frequency distributions of NTHA were compared (M1NL, M2NL, M3NL-1), the frequency information within 1-3 Hz was found to be lower in M3NL-1.

In the case of GM2, the highest FT peak was due to M2 at 2.27 Hz, M1 and M5 have similar peaks but shifted at 2.51 Hz and 1.80 Hz, respectively. It could be understood from the frequency of peak shear force amplitudes of the most critical models (i.e., M1NL, M2NL) that the structure behaves essentially in quasi-linear range. It is interesting to observe that dissipation between foundation system and surrounding soil present in M3NL-1 seems to be important enough to reduce sharply the peak shear force demand, which is discovered to occur due to a slight reduction of frequency content within 2-3 Hz range.

Looking at velocity time histories (Fig. 11(a) and (b)) the similarities in terms of shape and peak values between M1NL M2NL, and M5 and on the other side the differences with M3NL-1 were even more evident than for shear forces, suggesting that fixed base models and spring models overestimated the bridge response, not being able to catch the dissipation of the energy due to SSI. As it was expected, in case GM1, the more rigid system (M1NL) was the one

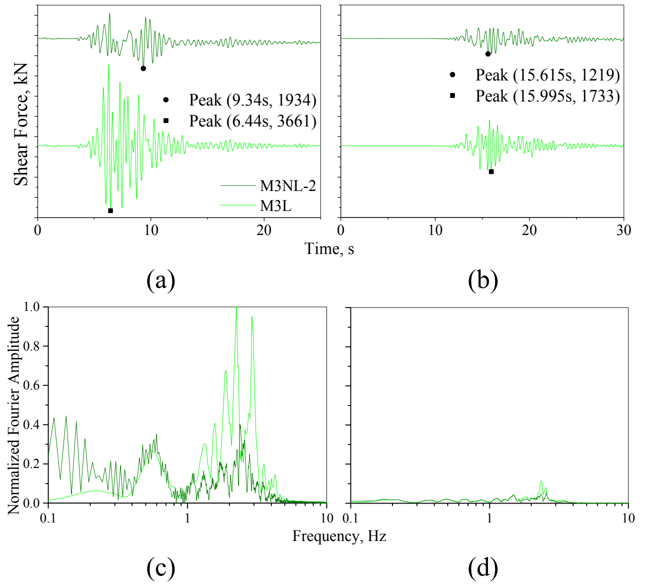

Fig. 12 Shear force-time histories (SFTHs) obtained as a function of linear and nonlinear soil domain in model M3. (a) SFTHs due to GM1, (b) SFTHs due to GM2, (c) normalized Fourier amplitude of SFTHs due to GM1, (d) normalized Fourier amplitude of SFTHs due to GM2

with higher velocity; however, this was not confirmed in the case of GM2 where M5 predominated.

It is worth mentioning the effect of the nonlinearity of soil on the response of the structure, which was done through comparing the differences in shear force and its FTs of the linear structure (piers), extracted from the models: M3L and M3NL-2. Such a comparison was provided in Fig. 12. It could be mentioned that due to soil nonlinearity there the peak shear force demand is reduced to approximately 50% and 70% of the linear demand under GM1 and GM2, respectively. When the response of M3NL and M3NL-2 (Fig. 10(a) and (b) vs Fig. 12(a) and (b)) was compared, it could be mentioned that the peak shear forces are 1300 kN and 1934 kN for GM1, and 966 kN and 1219 kN for GM2, respectively.

Moment-curvature responses were compared at the top and bottom of the 8th pier (see Fig. 13(a) and (b)) for M3NL-1 and M5 models under GM1. In the case of M3NL-1, the two curves were very similar and almost linear, indicating that all the effects of GM1 were dissipated by the soil-structure interaction at foundation level that worked as a filter for the structure. This was not the case for M5 that shows highly nonlinear response at the top of the pier, while the curve at the base of the pier was similar to M3NL-1. It indicated that the spring-dashpot model was not able to correctly replicate the nonlinear behavior of the soil and in particular, it's capacity of dissipating energy. A similar response was observed under GM2 in Fig. 13(c) and (d).

Finally, a nonlinear response at top and more linear response at bottom sections are justifiable when one considers the actual fixity conditions of the bridge piers which were monolithically connected to a very rigid deck at the top and more flexible foundation-soil system at the bottom.

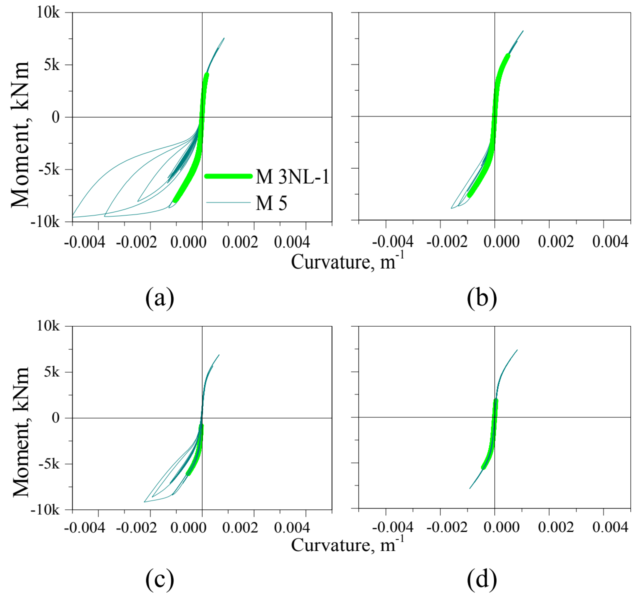

Fig. 13 Moment-curvature responses of Pier 8 under GM1, (a) top section and (b) bottom section; under GM2, (c) top section and (d) bottom section

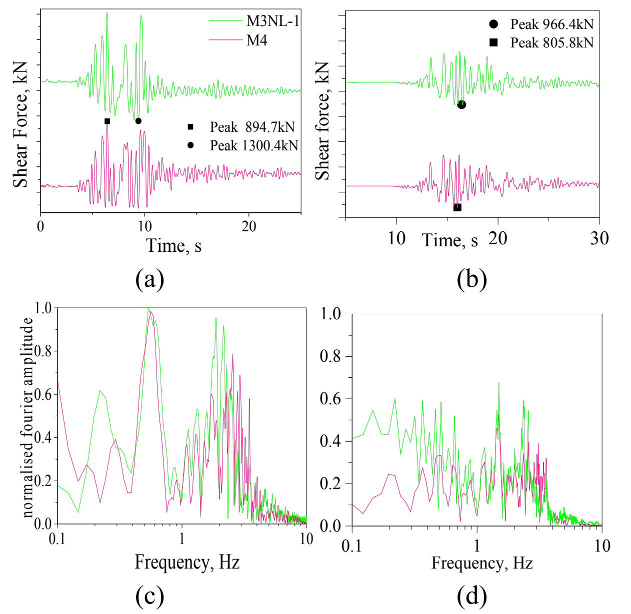

Fig. 14 Shear force time histories (SFTHs) obtained as a function of the abutment-backfill interaction. (a) SFTHs due to GM1, (b) SFTHs due to GM2, (c) normalized FAS of SFTHs due to GM1, (d) normalized FAS of SFTHs due to GM2

4.3 Effect of the presence of abutment-backfill interaction on the overall response

In this section, first, the impacts of abutment-backfill interaction were presented by comparing the results of M3NL-1 and M4 in terms of pier 8 shear force demands. Afterward, the performance of the simplified spring-dashpot model M6 was presented through a series of comparisons with the M4 model also encompassing the corresponding moment-curvature relations.

In Fig. 14, the comparisons of shear force demands were

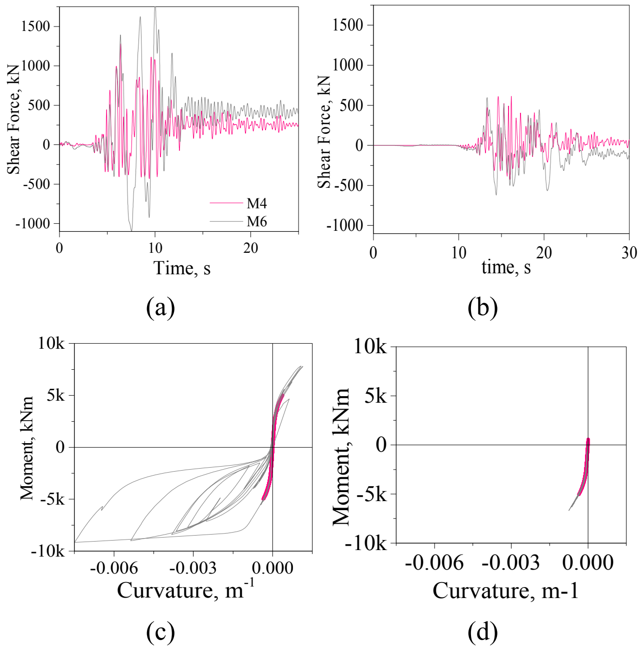

Fig. 15 Shear force time histories (SFTHs) obtained through fully coupled SSI model with abutment backfill (M4) and simplified spring-dashpot model (M6): (a) SFTHs due to GM1, (b) SFTHs due to GM2. Moment-curvature responses of Pier 8 top section: (c) under GM1, (d) under GM2

provided under GM1 and GM2. From Fig. 14(a), an already expected reduction in overall shear force demand was observed from a peak value of 1300 kN of M3NL-1 to 895 kN of M4 due to additional passive resistance provided by the backfill soil in case of GM1. Further investigations on Fig. 14(c) proves that the overall system got stiffer passing from M3NL-1 to M4, tending to amplify more the region of higher frequencies (i.e., 2-4 Hz) instead of around 2 Hz. This was because even reduced inelasticity on the pier elements. Furthermore, under GM2, the shear force also got reduced from M3NL-1 to M4 model in the time domain (in Fig. 14(c)) and in the frequency domain, there were sharper normalized peaks for the M4 model.

When the response of the simplified spring-dashpot model was investigated from the shear force response comparison provided in Fig. 15(a) and 15(b), it could be observed that M6 approach did not capture very well the effects observed in the fully-coupled M4, such as the residual shear force (i.e., under GM1; model M6 predicted 1.6 times higher residual shear forces. Clearly, higher residual shear force demand observed in the SFTHs were coupled with inelastic curvatures on the top sections as presented in Fig. 15(c) and 15(d), making the concluding observation being in parallel with the case M5 vs M3NL-1, without the presence of the abutments, presented in Fig. 13.

5. Conclusions

In Table 2, the mean values of the peak response under seven site-specific ground motions (in Fig. 5) for different modeling approaches are given.

Table 2 Mean values for selected engineering demand parameters corresponding to their peak responses

Engineering Demand Parameter	Models					
	M1L	M2L	M3L	M4	M5	M6
	M1NL	M2NL	M3NL-1 M3NL-2 M3NL-3			
Pier peak moment (kN.m)	61649	49039	46021	6593	9986	8717
	8595	8388	8074 12361 9447			
Pier peak shear force (kN)	9984	7889	7467	1054	1509	1416
	1464	1428	1334 2032 1563			
Pier residual differential shear force (kN)	Not available			264.2	360	580
	92	78.6	146 186.2 175			
Peak Curvature (1/m) %	-NA-			0.07	0.51	0.95
	0.05	0.45	0.18 -NA- 1.8			
Pier Maximum Drift ratio (%)	0.58	0.57	0.52	0.09	0.41	0.33
	0.26	0.2	0.23 0.15 1.0			

In summary, the points from 1 to 6 could be extracted from Table 2, which also synthesizes the main conclusions of the current study:

1. Due to their missing hysteretic damping, linear soil models presented in M1L, M2L, and M3L tend to amplify the rock outcrop motions significantly, thus ending up with significantly elevated levels of design actions. Therefore, even in the linear structural assessments, a nonlinear soil model should be adopted to obtain the elastic structural forces.
2. When one compares the response of M1L, M2L, and M3L, it could be stated that the inertial interaction plays the fundamental role as the response of M2L and M3L are very similar, simultaneously being significantly weaker than the one predicts by M1L. However, once the soil nonlinearity is introduced, it is observed that as the nonlinearity in the soil grows (i.e. higher intensity motion), the kinematic interaction acting in the frequency range 2-3 Hz loses its importance as the elevated hysteretic damping damps out of the content, thus M2NL provides very close estimates to M3NL-1. On the other hand, when the damping in soil is limited (i.e., lower intensity motion), kinematic interaction starts to be governing; thus M2NL provided a better match with M1NL, instead of M3NL-1.
3. Current day advanced engineering practice mostly considers the type of approach noted in M1NL, which takes into account two de-coupled nonlinear response histories being carried out for soil and structural domains. As compared to the coupled approach (M3NL-1), it is found out that such an approach is rather

overestimating the pier actions up to 25% for forces and 12% for deformations. As a matter of fact, it is found that when the input motion is used as the SSI motion (M2NL), considerably similar peak shear force/moment demand is present with respect to the fully coupled benchmark model (M3NL-1).

4. When the results of M3NL-2 (nonlinear soil and linear structure) and M3NL-1 (nonlinear soil and nonlinear structure) are investigated, it is observed that slight nonlinearity on the structure is present (the shear response is around 1.5 times smaller and the displacement response is around 1.5 times larger).

5. When the abutment-backfill interaction is considered (M4), it is found that due to the beneficial impact of caused by the passive resistance acting behind the abutments, the peak actions on the piers dropped about 20% with respect to the benchmark model (M3NL-1). Moreover, the increase in residual actions is found to be around 55%. Finally, the reduction in the deformation demand is found out to be 60%. It is important to note that the beneficial effect of the abutment-backfill interaction is found out to be much milder in the simplified spring-dashpot approach when the results of M6 is compared with M5 (Fig. 13 vs. Fig. 15).

6. Once the response of the simplified spring-dashpot models (i.e., M5 and M6) are compared with the response obtained in the fully coupled models (i.e., M3NL-1 and M4), it is found that simplified models tend to overestimate the peak moment demand by 0-10%, peak shear force demand by 10-25%, residual shear force demand by 55-60%, and maximum deformation demand by 43-72%. Curvature response at the deck level is higher in M5 and M6 models than M3NL-1 and M4 models. It can be argued that overall, the use of the simplified-dashpot system can be considered to stay in the safer side in terms of design aspect when assessing the effects of SSI.

It should be underlined that the findings of this work are limited to the response of a single bridge type (integral bridge with piled foundations) with the considered configuration (number of spans, pier/abutment dimensions, reinforcement configurations, etc.) under a single set of ground motions; hence it can't generalize to generic conditions with a similar level of confidence. On the other hand, the results may shed light to some extent into the configurations that are not considered and highlighted the need for further studies on other bridge typologies and with various configurations.

Acknowledgments

A significant part of this research was carried out while the first author (Sreya Dhar) was visiting Politecnico di Milano, under INTERWEAVE Project, Erasmus Mundus Program during 2014-2017. This work is a part of the Ph.D. thesis of the first author and the first author would like to thank the Ministry of Human Resources (MHRD) for the scholarship during her Ph.D. work.

References

Ahmadi, E., Khoshnoudian, F. and Hosseini, M. (2015), "Importance of soil material damping in seismic responses of soil-MDOF structure systems", *Soil. Found.*, **55**(1), 35-44. https://doi.org/10.1016/j.sandf.2014.12.003.

Ali, S.B. and Kim, D. (2017), "Wavelet analysis of soil-structure interaction effects on seismic responses of base-isolated nuclear power plants", *Earthq. Struct.*, **13**(6), 561-572. https://doi.org/10.12989/eas.2017.13.6.561.

API RP2A-WSD (2000), Recommended Practice for Planning, Designing and Constructing Fixed Offshore Platforms-Working Stress Design, American Petroleum Institute; Washington D.C, USA.

Argyroudis, S., Palaiochorinou, A., Mitoulis, S. and Pitilakis, D. (2016), "Use of rubberised backfills for improving the seismic response of integral abutment bridges", *Bull. Earthq. Eng.*, **14**(12), 3573- 3590. https://doi.org/10.1007/s10518-016-0018-1.

Ariyarathne, P., Liyanapathirana, D.S. and Leo, C.J. (2013). "Comparison of different two-dimensional idealizations for a geosynthetic-reinforced pile-supported embankment", *Int. J. Geomech.*, **13**(6), 754-768. https://doi.org/10.1061/(ASCE)GM.1943-5622.0000266.

Arockiasamy, M., Butrieng, N. and Sivakumar, M. (2004), "State-of-the-art of integral abutment bridges: Design and practice", *J. Bridge Eng.*, **9**, 497-506. https://doi.org/10.1061/(ASCE)1084-0702(2004)9:5(497).

Arsoy, S., Barker, R.M. and Duncan, M.J. (2002), "Experimental and analytical investigations of the piles and abutments of integral bridges", Virginia Tech. Research Counsel, FHWA/NTRC 02-CR6, Charlottesville, VA.

Boulanger, R.W., Curras, C.J., Kutter, B.L., Wilson, D.W. and Abghari, A. (1999), "Seismic soil-pile-structure interaction experiments and analysis", *J. Geotech. Eng.*, **125**(9), 750-759. https://doi.org/10.1061/(ASCE)1090-0241(1999)125:9(750).

Brødbæk, K.T., Møller, M., Sørensen, S.P.H. and Augustesen, A.H. (2009), "Review of p-y relationships in cohesionless soil", DCE Technical Reports No. 57, Department of Civil Engineering, Aalborg University.

Caltrans (2013), Seismic Design Criteria, California Department of Transportation Version 1.7.

Carvajal Uribe, J.C. (2011), "Seismic embankment-abutment-structure interaction of integral abutment bridges", Doctoral Dissertation, University of British Columbia.

Clough, R. and Penzien, J. (2003), *Dynamics of Structures*, 3rd Edition, Computers and Structures Inc., Berkeley, California.

Conboy, D. and Stoothoff, E. (2005), "Integral abutment design and construction: The New England experience", *The 2005FHWA Conference, Integral Abutment and Jointless Bridges (IAJB 2005)*, Baltimore, MD.

Darendeli, M.B. (2001), "Development of a new family of normalized modulus reduction and material damping curves", Ph.D. Thesis, University of Texas, Austin, Texas.

Dhar, S. (2018), "Suitability of numerical modelling approach of an Integral bridge for strengthening of RC pile foundation using SSI", Ph.D. Thesis, Indian Institute of Technology Guwahati, India.

Dhar, S. and Dasgupta, K. (2019a), "Seismic analysis of an integral bridge with retrofitted RC pile foundation in different foundation soils using simplified SSI", *7th International Conference on Earthquake Geotechnical Engineering*, Paper No. 11132, Roma, Italy.

Dhar, S. and Dasgupta, K. (2019b), "Seismic soil structure interaction for integral abutment bridges: a review", *Transp. Infrastruct. Geotech.*, 1-19. https://doi.org/10.1007/s40515-019-00081-y.

Dhar, S. and Dasgupta, K. (2019c), "Comparison of modal behaviour of integral abutment bridge with and without soil-structure interaction", Eds. Rao, A., Ramanjaneyulu, K.. Recent Advances in Structural Engineering, **2**, Lecture Notes in Civil Engineering.

Dhar, S., Özcebe, A.G. and Dasgupta, K. (2017), "Comparison between two modeling aspects to investigate seismic soil structure interaction in a jointless bridge", *13th International Conference on Vibration Problems (ICOVP)*, Paper No. 201, Guwahati, India.

Dhar, S., Özcebe, A.G., Dasgupta, K., Dey, A., Paolucci, R. and Petrini, L. (2016), "Nonlinear dynamic soil-structure interaction effects on the seismic response of a pile-supported integral bridge structure", *6th International Conference on Recent Advances in Geotechnical Earthquake Engineering and Soil Dynamics*, Paper No. 141, New Delhi, India.

Douglas, B.M. and Reid, W.H. (1982), "Dynamic test and system identification of bridges", *J. Struct. Div*., **108**(ST10), 2295-2312.

Elgamal, A. (2010), "Calibrated 3D computational modeling of soil-structure systems and liquefaction scenarios", *International Conferences on Recent Advances in Geotechnical Earthquake Engineering and Soil Dynamics*, 1.

Elgamal, A., Yan, L., Yang, Z. and Conte, J.P. (2008), "Three-dimensional seismic response of Humboldt Bay Bridge-Foundation-Ground system", *J. Struct. Eng*., **134**(7), 1165-1176. https://doi.org/10.1061/(ASCE)0733-9445(2008)134:7(1165).

Erhan, S. and Dicleli, M. (2017), "Parametric study on the effect of structural and geotechnical properties on the seismic performance of integral bridges", *Bull. Earthq. Eng.*, **15**(10), 4163-4191. https://doi.org/10.1007/s10518-017-0123-9.

Figini, R. and Paolucci, R. (2017), "Integrated foundation-structure seismic assessment through non-linear dynamic analyses", *Eqrthq. Eng. Struct. Dyn*., **46**(3), 349-367. https://doi.org/10.1002/eqe.2790.

Filippou, F.C., Popov, E.P. and Bertero, V.V. (1983), "Effects of bond deterioration on hysteretic behavior of reinforced concrete joints", Report EERC 83-19, Earthquake Engineering Research Center, University of California, Berkeley.

Finn, W. L. (2004), "Characterizing pile foundations for evaluation of performance based seismic design of critical lifeline structures", *13th World Conference on Earthquake Engineering*.

Ganjavi, B., Bararnia M. and Hajirasouliha I. (2018), "Seismic response modification factors for stiffness degrading soil-structure systems", *Struct. Eng. Mech.*, **68**(2), 159-170. https://doi.org/10.12989/sem.2018.68.2.159.

Gazetas, G. (1991), "Formulas and charts for impedances of surface and embedded foundations", *J. Geotech. Eng.*, **117**(9), 1363-81. https://doi.org/10.1061/(ASCE)0733-9410(1991)117:9(1363).

Gazetas, G. and Dobry, R. (1984), "Horizontal response of piles in layered soil", *J. Geotech. Eng. Div.*, **110**(1), 20-40. https://doi.org/10.1061/(ASCE)0733-9410(1984)110:1(20).

Goel, R.K. (1997), "Earthquake characteristics of bridges with integral abutments", *J. Struc. Eng.*, **123**(11), 1435-1443. https://doi.org/10.1061/(ASCE)0733-9445(1997)123:11(1435).

Granas, J.L. (2016), "Undrained lateral soil response of offshore monopile in layered soil", M. Tech Thesis, Dept. of Civ. & Transport Eng., NTNU.

Greimann, L.F., Yang, P.S. and Wolde-Tinsae, A.M. (1986), "Nonlinear analysis of integral abutment bridges", *J. Struct. Eng.*, **112**(10), 2263-2280. https://doi.org/10.1061/(ASCE)0733-9445(1986)112:10(2263).

Guo, J., Tang, Z., Chen, S. and Li, Z. (2016), "Control strategy for the substructuring testing systems to simulate soil-structure interaction", *Smart Struct. Syst.*, **18**(6), 1169-1188. http://dx.doi.org/10.12989/sss.2016.18.6.1169.

Highways Agency (2003), BA 42/96: The Design of Integral Bridges, HMSO, London, UK.

Holzer, T.L., Padovani, A.C., Bennett, M.J., Noce, E.T. and Tinsley, J.C. (2005), "Mapping NEHRP V_{S30} site classes", *Eqrthq. Spectra*, **21**(2), 1-18. https://doi.org/10.1193/1.1895726.

Horvath, J.S. (2000), "Integral-abutment bridges: problems and innovative solutions using EPS geofoam and other geosynthetics", Research Report No. CE/GE-00, 2, Manhattan College, School of Engineering, NY.

Hoseini, S.S., Ghanbari, A., Davoodi, M. and Kamal, M. (2019), "The effect of foundation soil behavior on seismic response of long bridges", *Geomech. Eng.*, **17**(6), 583-595. https://doi.org/10.12989/gae.2019.17.6.583.

Jiang, S., Du, C. and Sun, L. (2018), "Numerical analysis of sheet pile wall structure considering soil-structure interaction", *Geomech. Eng.*, **16**(3), 309-320. https://doi.org/10.12989/gae.2018.16.3.309.

Karakas, A.I., Ozgan, K. and Daloglu, A.T. (2018), "Soil-structure interaction effects on seismic behavior of a hyperbolic cooling tower using three-parameter Vlasov foundation model", *Earthq. Struct.*, **14**(1), 085-94. https://doi.org/10.12989/eas.2018.14.1.085.

Karantzikis, M. and Spyrakos, C.C. (2000), "Seismic analysis of bridges including soil-abutment interaction", *Proceedings of the 12th World Congress on Earthquake Engineering*, Paper No. 2471.

Kim, W., Jeong, Y. and Lee, J. (2018), "A design approach of integral-abutment steel girder bridges for maintenance", *Steel Compos. Struct*. **26**(2), 227-239. https://doi.org/10.12989/scs.2018.26.2.227.

Kontoe, S., Zdravković, L., Potts, D.M. and Salandy, N.E. (2007), "The Domain Reduction Method as an advanced boundary condition", *4th International Conference on Earthquake Geotechnical Engineering*. Paper No. 1231. Greece.

Kotsoglou, A.N. and Pantazopoulou, S.J. (2009), "Assessment and modeling of embankment participation in the seismic response of integral abutment bridges", *Bull. Earthq. Eng*., **7**(2), 343-361. https://doi.org/10.1007/s10518-009-9103-z.

Kuhlemeyer, R.L. and Lysmer, J. (1973), "Finite element method accuracy for wave propagation problems", *J. Soil Mech. Found. Div*., ASCE, **99**, 421-427.

Lee, J., Kim, W., Kim, K., Park S. and Jeon, Y. (2016), "Strengthened and flexible pile-to-pilecap connections for integral abutment bridges", *Steel Compos. Struct*., **20**(4), 731-748. https://doi.org/10.12989/scs.2016.20.4.731.

Lysmer, J. and Kuhlemeyer, R.L. (1969), "Finite dynamic model for infinite media", *J. Eng. Mech. Div*., **95**(EM4), 859-877.

Mazzoni, S., McKenna, F., Scott, H.M. and Fenves, G.L. (2007), "The OpenSees command language manual", v6.0 http://opensees.berkeley.edu, Pacific Earthquake Engineering Research Center, University of California, Berkeley.

McKenna, F. and Fenves, G.L. (2008), "Using the OpenSees interpreter in parallel computers", University of California, Berkeley, NEESit; TN-2007-16, v1.0.

McKenna, F., Fenves, G.L. and Scott, M.H. (2000), "Open system for earthquake engineering simulation", University of California, Berkeley, CA.

Messioud, S., Sbartai, B. and Dias, D. (2016), "Seismic response of a rigid foundation embedded in a viscoelastic soil by taking into account the soil-foundation interaction", *Struct. Eng. Mech*., **58**(5), 887-903. https://doi.org/10.12989/sem.2016.58.5.887.

Mirrezaei, S.S., Barghian, M., Ghaffarzadeh, H. and Farzam, M. (2016), "Retrofitting of steel pile-abutment connections of integral bridges using CFRP", *Struct. Eng. Mech*., **59**(2), 209-226. http://dx.doi.org/10.12989/sem.2016.59.2.209.

Mitoulis, S.A. (2016), "Some open issues in the seismic design of bridges to Eurocode 8-2", *Chall. J. Struct. Mech.*, **2**(1), 7-13. http://dx.doi.org/10.20528/cjsmec.2016.02.002

Mitoulis, S.A., Palaiochorinou, A., Georgiadis, I. and Argyroudis, S. (2016), "Extending the application of integral frame abutment bridges in earthquake-prone areas by using novel isolators of recycled materials", *Earthq. Eng. Struct. Dyn.*, **45**(14), 2283-2301. https://doi.org/10.1002/eqe.2760.

Mokwa, R.L. (1999), "Investigation of the resistance of pile caps to lateral spreading", Ph.D. Thesis, Dept. of Civil Engineering, Virginia Polytechnic Institute and State University, Blacksburg, VA.

Monkul, M.M. (2008), "Validation of practice oriented models and influence of soil stiffness on lateral pile response due to kinematic loading", *Marine Geores. Geotech.*, **26**(3), 145-159. https://doi.org/10.1080/10641190802138118.

Naderi, M. and Zekavati, M. (2018), "Assessment of seismic behavior stone bridge using a finite element method and discrete element method", *Earthq. Struct.*, **14**(4), 297-303. https://doi.org/10.12989/eas.2018.14.4.297.

Neuenhofer, A. and Filippou, F.C. (1998), "Geometrically nonlinear flexibility-based frame finite element", *J. Struct. Eng.*, **124**(6), 704-711. https://doi.org/10.1061/(ASCE)0733-9445(1998)124:6(704).

Ostadan, F., Deng, N. and Roesset, J.M. (2004), "Estimating total system damping for soil-structure interaction systems", *Third UJNR Workshop on Soil-Structure Interaction*, Menlo Park, California.

Paolucci, R., Figini, R. and Petrini, L. (2013), "Introducing dynamic nonlinear soil-foundation-structure interaction effects in displacement-based seismic design", *Earthq. Spectra*, **29**(2), 475-496. https://doi.org/10.1193/1.4000135.

Park, M.C. and Nam, M.S. (2018), "Behavior of integral abutment bridge with partially protruded piles", *Geomech. Eng.*, **14**(6), 601-614. https://doi.org/10.12989/gae.2018.14.6.601.

Petersen, M.D., Frankel, A.D., Harmsen, S.C., Mueller, C.S., Haller, K.M., Wheeler, R.L., Wesson, R.L., Zeng, Y., Boyd, O.S., Perkins, D.M. and Luco, N. (2008), "Documentation for the 2008 update of the United States national seismic hazard maps", U.S.G.S. Open-File Report 2008, 1128-1161.

Petursson, K. and Kerokoski, P. (2011), "Monitoring and analysis of abutment-soil interaction of two integral bridges", *J. Bridge Eng.*, **18**(1), 54-64. https://doi.org/10.1061/(ASCE)BE.1943-5592.0000314.

Prevost, J.H. (1985), "A simple plasticity theory for fFrictional cohesionless soils", *Soil Dyn. Earthq. Eng.*, **4**(1), 9-17. https://doi.org/10.1016/0261-7277(85)90030-0.

Quinn, B.H. and Civjan, S.A. (2016), "Parametric study on effects of pile orientation in integral abutment bridges", *J. Bridge Eng.*, 04016132. https://doi.org/10.1061/(ASCE)BE.1943-5592.0000952.

Scott, B.D., Park, R. and Priestley, M.J.N. (1982), "Stress-strain behavior of concrete confined by overlapping hoops at low and high strain rates", *J. Am. Concrete Inst.*, **79**, 13-27.

Shamsabadi, A., Rollins, K.M. and Kapuskar, M. (2007), "Nonlinear soil-abutment-bridge structure interaction for seismic performance-based design", *J. Geotech. Geoenv. Eng.*, **136**(6), 707-720. https://doi.org/10.1061/(ASCE)1090-0241(2007)133:6(707).

Smerzini, C., Galasso, C., Iervolino, I. and Paolucci, R. (2014), "Ground motion record selection based on broadband spectral compatibility", *Earthq. Spectra*, **30**(4), 1427-1448. https://doi.org/10.1193/052312EQS197M.

Smerzini, C., Paolucci, R., Galasso, C. and Iervolino, I. (2012), "Engineering ground motion selection based on displacement-spectrum compatibility", *Proceedings of the 15th World Conference on Earthquake Engineering*, Paper no. 2354, Lisbon, Portugal.

Thanoon, W.A., Abdulrazeg, A.A., Noorzaei, J., Jaafar, M.S. and Kohnehpooshi, O. (2011), "Soil structure interaction for integral abutment bridge using spring analogy approach", *IOP Conference Series: Materials Science and Engineering*, **17**(1), 012035.

Tsinidis, G., Papantou, M. and Mitoulis, S. (2019), "Response of integral abutment bridges under a sequence of thermal loading and seismic shaking", *Earthq. Struct.*, **16**(1), 11-28.

Wasserman, E. and Walker, J. (1996), *Integral Abutments for Steel Bridges*, TDOT, TN.

Weakley, K. (2005), "VDOT integral bridge design guidelines", *The 2005FHWA Conference, Integral Abutment and Jointless Bridges (IAJB 2005)*, Baltimore, MD, 61-70.

Zhang, J. and Makris, N. (2002), "Seismic response analysis of highway overcrossings including soil-structure interaction", *Earthq. Eng. Struct. Dyn.*, **31**, 1967-1991. https://doi.org/10.1002/eqe.197.

Zhang, Y., Conte, J.P., Yang, Z., Elgamal, A., Bielak, J. and Acero, G. (2008), "Two dimensional nonlinear earthquake response analysis of a bridge-foundation ground system", *Earthq. Spectra*, **24**(2), 343-386. https://doi.org/10.1193/1.2923925.

Zhao, Q., Vasheghani-Farahani, R. and Burdette, E.G. (2011), "Seismic analysis of integral abutment bridges including soil-structure interaction", *Structures Congress 2011,* 289-303.

AT